CASE REPORT

Protein-Losing Enteropathy Associated With Egg Allergy in a 5-Month-Old Boy

M Kondo,[1] T Fukao,[1,2] K Omoya,[1] N Kawamoto,[1] M Aoki,[1] T Teramoto,[1] H Kaneko,[1] N Kondo[1]

[1]Department of Pediatrics, Graduate School of Medicine, Gifu University, Gifu, Japan
[2]Medical Information Science Division, United Graduate School of Drug Discovery and Medical Information Sciences, Gifu University, Gifu, Japan

Abstract

Protein-losing enteropathy (PLE), the manifestation of a diverse set of disorders, is characterized by excessive loss of plasma proteins into the affected portions of the gastrointestinal tract, and this results in hypoalbuminemia. A 5-month-old breastfed boy presented severe PLE with hypogammaglobulinemia, hypocalcemia, and hypomagnesemia induced by an egg allergy. He developed hypocalcemic convulsions. The diagnosis of PLE was confirmed by elevated fecal $_1$-antitrypsin clearance and a positive finding on a protein-losing scintigram. His allergy to egg delivered through maternal milk was confirmed as the cause of PLE, since the mother's elimination of egg from her diet improved his condition and maternal egg challenge provoked symptoms of diarrhea, vomiting, and elevated $_1$-antitrypsin clearance. At the time of writing, he is 22 months old and has experienced no further episodes after the elimination of egg-containing food.

Key words: Protein-losing enteropathy (PLE). Hypocalcemia. Egg allergy. Food challenge.

Resumen

La enteropatía de pérdida de proteínas (EPP), la manifestación de varios conjuntos de trastornos, se caracteriza por la pérdida excesiva de proteínas séricas en los tramos afectados del aparato gastrointestinal, dando lugar a la hipoalbuminemia. Un niño de 5 meses alimentado con lactancia materna presentó EPP grave con hipogammaglobulinemia, hipocalcemia e hipomagnesemia inducidas por una alergia al huevo. El niño presentó convulsiones por hipocalcemia. El diagnóstico de EPP se confirmó mediante la elevada eliminación de $_1$-antitripsina en las heces y el resultado positivo en una gammagrafía de pérdida de proteínas. La alergia al huevo, que procedía de la ingesta de la leche materna, se confirmó como la causa de la EPP, ya que cuando la madre eliminó el huevo de su dieta el estado del niño mejoró, pero la prueba de provocación con huevo de la madre ocasionaba la aparición de los síntomas de diarrea, vómitos y una elevada eliminación de $_1$-antitripsina . En el momento en que se escribe este documento, el niño tiene 22 meses y no ha experimentado ningún otro episodio después de la eliminación de alimentos que contuvieran huevo.

Palabras clave: Enteropatía de pérdida de proteínas (EPP). Hipocalcemia. Alergia al huevo. Prueba de provocación alimentaria.

Introduction

Protein-losing enteropathy (PLE) has been associated with many disorders occurring at different anatomic sites in the gastrointestinal tract. Any process that leads to a profound leakage of proteins from the gastrointestinal tract can lead to PLE but there are 3 main mechanisms that are responsible: 1) lymphatic obstruction, such as primary intestinal lymphangiectasia, cardiac diseases, and lymphoma; 2) erosions and ulcerations, such as erosion of the esophagus and ulcerative colitis; and 3) intestinal permeability (leakage), such as is found in celiac disease and Henoch-Schönlein purpura, [1-3]. Food-allergies are attributable to the adverse immune response to dietary proteins and account for numerous gastrointestinal disorders of childhood [3]. Eosinophilic gastroenteritis and dietary protein enteropathy have been reported to cause PLE [3].

We report on a 5-month-old boy who had PLE caused by allergy to egg proteins that had arrived through maternal milk. He developed hypocalcemic convulsions.

Case Description

A 5-month-old boy was hospitalized with the chief complaint of afebrile convulsions 3 times a day. He had been exclusively breastfed until he started eating rice porridge 10 days earlier. His grandmother had pointed out his loose stools 2 weeks before hospitalization and his mother reported that he had had diarrhea (3 times per day) and regurgitated milk (several times per day) for 3 days prior to admission. He drank well and had been cheerful. His parents did not recognize his change, which included edema. His developmental milestones were within the normal range. His height was 69.5 cm and body weight was 7.8 kg. On admission, he was conscious, slightly edematous with pretibial pitting edema, periorbital edema, and was mildly hypotonic. He had no apparent dermatitis. Laboratory data on admission (table) showed remarkable hypoproteinemia including hypogammaglobulinemia (total protein, 2.8 g/dL; albumin, 1.9 g/dL; immunoglobulin [Ig] G, 31 mg/dL; IgM, 19 mg/dL; IgA 7 mg/dL). In addition, serum calcium (3.8 mg/dL; corrected for serum albumin, 5.4 mg/dL) and magnesium (0.8 mg/dL) levels were very low; serum sodium, potassium, and chloride levels were within normal ranges. Lymphocytopenia (<1000/ L) was noted. The C-reactive protein level was within the normal range. Urine analysis showed neither proteinuria nor hematuria.

Analyses of cerebrospinal fluid, an electroencephalogram, computed tomography and magnetic resonance imaging of the brain showed no abnormalities. Thus, his recurrent convulsions were considered to be due to severely low calcium and magnesium levels. Convulsions occurred twice after admission. The patient was given intravenous calcium, magnesium, and albumin; after 7 days, calcium and magnesium levels became normal, after which convulsions did not recur.

Since proteinuria was not observed, a loss of proteins into the gastrointestinal tract was suspected as the cause of hypoproteinemia. Fecal occult blood was repeatedly positive and $_1$-antitrypsin clearance was 400 mL/d (normal range, below 13 mL/d). His stool culture was negative and a rotavirus antigen test was negative. May–Giemsa staining of the stool revealed no eosinophils. A protein-losing scintigram using technetium 99m (99mTc)-labeled human serum albumin demonstrated leakage into the small intestine. Based on these findings, we diagnosed PLE.

The infant's serum IgE level was slightly high (22 U/mL). The egg-white and egg-yolk–specific IgE levels measured by CAP system radioallergosorbent testing (RAST) (Phadia, Uppsala, Sweden) were 1.2 kU/L and 1.1 kU/L, respectively, whereas other allergen-specific IgE antibodies (to milk, wheat, rice, soybean, mites, house dust) were not detected. Prick tests for egg-white and egg-yolk were positive but tests for other foods (milk, soybean, rice, wheat) were negative. In intracellular interleukin (IL) 4 and interferon (IFN) staining of $CD4^+$ cells, the percentages of type 1 helper T cells (T_H1) (IFN- positive, IL-4 negative) and T_H2 cells (IFN- negative, IL-4 positive) were both highly elevated to 28.5% and 4.8%, respectively, on admission in comparison with age-matched controls (T_H1, 2.02% [SD, 1.12 %]; T_H2, 0.33% [SD, 0.18%]) [4]. The T_H1 and T_H2 percentages decreased gradually to 5.23% and 0.28%, respectively, on discharge.

After admission, oral food intake including breastfeeding was stopped and total parenteral nutrition was undertaken for 10 days. Four days before breastfeeding was restarted, elimination of egg-containing foods from his mother's diet was started. Then maternal milk and additional formula milk feeding was restarted. He had no vomiting or diarrhea, and his serum protein levels increased gradually (on the 50th hospital day: total proteins, 5.3 g/dL; albumin, 4.1 g/dL; IgG, 197 mg/dL; IgM, 71 mg/dL; and IgA 28, mg/dL). Fecal $_1$-antitrypsin clearance decreased to the normal range. The second protein-losing scintigram (1 month after the first scintigram) did not detect leakage of the labeled albumin into the intestine.

A food challenge test for egg through maternal milk was started on the 50th hospital day. His mother took 1 whole boiled egg every 2 days and continued to breastfeed. The boy was well until the second challenge when he vomited 3 times. Egg was again eliminated from the mother's diet. Positive occult blood in the stool was noted for 3 days after the second challenge. $_1$-antitrypsin clearance in the stool was elevated again to 360 mL/d; however the clearance became normal within 2 weeks after the challenge. He was discharged at 120 days.

At age 22 months, he thrives with egg-containing foods eliminated from his diet. No other food restriction has been necessary. He has experienced no further episodes of PLE and has had no apparent symptoms of gastrointestinal food allergy.

Discussion

We have presented a case of PLE caused by egg allergy. Diagnosis of PLE was confirmed by hypoalbuminemia, elevated $_1$-antitrypsin clearance in stool, and a positive protein-losing scintigram using 99mTc-labeled human serum albumin. Egg allergy was confirmed as the cause of PLE by 1) improvement of the boy's condition with the first period of elimination of eggs from the mother's diet; 2) diarrhea and vomiting, with elevated $_1$-antitrypsin clearance, provoked by the egg challenge through maternal milk; 3) further improvement with re-elimination of egg-containing foods from the mother's diet.

A positive egg-white and egg-yolk IgE RAST and positive prick test for those foods indicated that the patient was sensitized to egg through maternal milk since he had never taken egg-containing food directly. Egg allergens, as well as cow's milk and wheat allergens, have been detected in breast milk as little as 2 to 6 hours after maternal intake and can be detected as long as 4 days later [5-7]. We therefore considered egg allergy as one of the causes of PLE. There are several gastrointestinal food-allergic disorders of infancy and childhood [3]. Our patient's PLE could have been dietary protein enteropathy [3], but an endoscopic examination and biopsy were not performed in this case. Usually, these gastrointestinal food-allergic disorders,

Table. Comparison of the Present Protein-Losing Enteropathy Case With a Previously Reported Case [9]

	Present Case	Previous Case [9]
Onset	5 months	4 months
Feeding	breastfed	milk-formula–fed[a]
Diarrhea		
Onset	4.5 months	3 months
Frequency	3 times/d	5-6 times/d
Weight gain	good	good
General condition	good	good
Convulsions	present	present
Laboratory data on admission		
Total protein, g/dK	2.8	2.8
Albumin, g/dL	1.9	1.6
IgG, mg/dL	31	69
IgA, mg/dL	7	11.8
IgM, mg/dL	19	35
IgE, U/mL	22	220
Sodium, mEq/L	136	125
Potassium, mEq/L	3.9	3.2
Chloride, mEq/L	108	99
Calcium, mg/dL	3.8	4.6
Magnesium, mg/dL	0.8	0.7
White blood cells, per L	6440	NR
Lymphocytes, per L	943	NR
$CD3^+$, per L	366	1366
$CD4^+$, per L	134	528
$CD8^+$, per L	269	1157
$CD19^+$, per L	359	NR
T_H1, % in $CD4^+$ cells	28.5%	NR
T_H2, % in $CD4^+$ cells	4.8%	NR
IgE CAP-RAST		
Egg white, kU/L	1.4	markedly increased[b]
Egg yolk, kU/L	1.1	markedly increased[b]
Milk, kU/L	<0.34	markedly increased[b]
Histamine releasing test	no information	egg positive
Prick test	egg positive	NR
Protein-losing scintigram	positive	positive
Lymphoscintigram	not done	dilated
Egg elimination	effective	effective
Egg challenge	positive	not done

Abbreviations: Ig, immunoglobulin; T_H1 and T_H2, types 1 and 2 helper T cells; NR, not reported.
[a] This patient breastfed for the first few days.
[b] In their report, Hamada et al [9] did not report exact values; they used the phrase "RAST values for milk and egg were markedly increased" (p. 687).

except for immediate gastrointestinal hypersensitivity, are non-IgE-mediated but are associated with T cell responses [8]. We consider that the presence of a positive IgE antibody and prick test for egg protein does not exclude the presence of non-IgE-mediated enteropathy with T cell responses. In fact, activation of T_H1 and T_H2 cells were suspected by the fact that the percentages those cells in peripheral blood $CD4^+$ lymphocytes were very high on admission and were normalized on discharge from the hospital.

The boy presented not only hypoalbuminemia but also hypogammaglobulinemia, lymphocytopenia, and hypocalcemia/hypomagnesemia. In general, a low immunoglobulin level and lymphocytopenia are common in PLE that is caused by lymphatic obstruction but rare in PLE caused by other mechanisms. In this context, this patient was suspected of having PLE caused by lymphatic obstruction.

We located a case report of a 4-month-old boy whose clinical presentation was very similar to our patient's (table) [9]. That infant also had hypogammaglobulinemia, hypocalcemia, and hypomagnesemia with recurrent convulsions. He was diagnosed as having intestinal lymphangiectasia accompanying PLE by means of a protein-losing scintigram and lymphoscintigram.

However, although tests for IgE antibodies were positive for both egg and milk, a histamine-releasing test was positive only for egg. He was on hyperalimentation for the first month and thereafter elimination of egg from his diet was continued. His PLE condition, including laboratory findings, normalized completely 6 months later. A challenge test for egg was not performed in that case, but the elimination of egg as well as medium-chain triglyceride milk improved his condition. We did not perform a lymphoscintigram for our patient, but the laboratory data were consistent with those for lymphatic obstruction, and in general our case is consistent with the previous report. We speculate that some patients with dietary protein enteropathy may have lymphatic obstruction or a similar pathological condition which excretes gammaglobulin, calcium, and magnesium into the intestinal tract.

In summary, we report a rare case of infantile egg allergic enteropathy through maternal milk which caused severe PLE with hypocalcemia and hypomagnesemia resulting in afebrile convulsions in an infant.

Acknowledgment

The immunological studies referred to in this report were in part funded by the Research and Development Program for New Bio-industry Initiatives (2005-2009) of the Bio-oriented Technology Research Advancement Institution (BRAIN), Japan.

References

1. Gracey M, Anderson CM. Intestinal lymphangiectasia and other causes of protein-losing gastroenteropathies. In: Gracey M, Burke V, eds. Pediatric Gastroenterology and Hepatology. Oxford: Blackwell Scientific Publications. 1993. p. 439–40.
2. Strober W, Wochner RD, Carbine PP, Waldmann TA. Intestinal lymphangiectasia. A protein-losing gastroenteropathy with hypogammaglobulinemia, lymphocytopenia and impaired homograft rejection. J Clin Invest. 1967;46:1643–56.
3. Sicherer SH. Clinical aspects of gastrointestinal food allergy in childhood. Pediatrics. 2003;111:1609-16.
4. Kawamoto N, Kaneko H, Takemura M, Seishima M, Sakurai S, Fukao T, Kasahara K, Iwasa S, Kondo N. Age-related changes in intracellular cytokine profiles and Th2 dominance in allergic children. Pediatr Allergy Immunol. 2006;17:125-33.
5. Cant A, Marsden RA, Kilshaw PJ. Egg and cows' milk hypersensitivity in exclusively breast fed infants with eczema, and detection of egg protein in breast milk. Br Med J (Clin Res Ed). 1985;291:932-5.
6. Stuart CA, Twiselton R, Nicholas MK, Hide DW. Passage of cows' milk protein in breast milk. C into human breast milk. Acta Paediatr Scand. 1987;76:453-6.
8. Hauer AC, Breese EJ, Walker-Smith JA, MacDonald TT. The frequency of cells secreting interferon-gamma and interleukin-4, -5, and -10 in the blood and duodenal mucosa of children with cow's milk hypersensitivity. Pediatr Res. 1997;42:629-38.
9. Hamada A, Kondoh T, Kamei T, Tominaga N, Tsuru A, Matsumoto T, Matsuzaka T, Moriuchi H. Protein-losing enteropathy complicated with recurrent convulsions and developmental delay in a 4-month-old boy. Pediatr Int. 2002; 44:686-9.

Manuscript received June 21, 2007; accepted for publication August 20, 2007.

Toshiyuki Fukao

Department of Pediatrics
Graduate School of Medicine, Gifu University
Yanagido1-1, Gifu 501-1194, Japan
E-mail: toshi-gif@umin.net

Induction of α1 and α2 gene expression in selective immunoglobulin A deficiency

HIROKO SUZUKI, HIDEO KANEKO, JIN RONG, NORIO KAWAMOTO, TSUTOMU ASANO, EIKO MATSUI, KIMIKO KASAHARA, TOSHIYUKI FUKAO and NAOMI KONDO

Department of Pediatrics, Graduate School of Medicine, Gifu University, Gifu, Japan

Received December 3, 2007; Accepted January 24, 2008

Abstract. Immunoglobulin A deficiency (IgAD) is the most common immunodeficiency, but the pathogenesis of most cases of IgAD is poorly understood. The gene and protein expression levels of members of the IgA subclasses in IgAD patients were analyzed by a reverse transcriptase (RT)-PCR method that could differentiate between α1 and α2 gene expression. Three selective, 5 partial and 2 secondary IgAD patients were examined. Peripheral blood mononuclear cells which were unstimulated or stimulated with TGF-ß1 and PMA for 24 h were cultured. The IgA1/IgA2 expression ratios were measured by zone densitometry. Three bands appeared (the α1 and α2 genes and a hetero-duplex formation), owing to the difference of 39 bases between α1 and α2 mRNAs. In the controls, there were no significant differences in the IgA1/IgA2 ratios between unstimulated and stimulated cells. In selective IgAD patients, both α1 and α2 gene expression was induced following stimulation, and α1 gene expression was induced more dominantly than in the other IgAD patients following stimulation. Based on our results, suppression of α1 gene expression may be related to the pathogenesis of IgAD.

Introduction

Human immunoglobulin A (IgA) is the major type of secreted antibody consisting of two subclasses, IgA1 and IgA2. The ratios of IgA1/IgA2 in secretions vary, and the functions of IgA1 and IgA2 in immune response remain unclear (1,2).

IgA deficiency (IgAD) is the most common immunodeficiency. The prevalence in Caucasians is approximately 1 in 500, while the prevalence in the Japanese is much lower; approximately 1 in 18,000 (3-5). IgAD is associated with a variety of infections, allergies, autoimmune disorders, gastrointestinal diseases, malignancies, endocrinopathies, neurological diseases and genetic disorders (3,6). IgAD is often associated with other forms of immunoglobulin deficiencies, including IgG subclasses and IgE deficiency (7-10). Certain IgAD patients have an α gene deletion, but the pathogenesis of some cases of IgAD is still poorly understood. Recently, it has become clear that certain common variable immunodeficiency and IgAD patients possess mutations in TNFRSF13B [encoding TACI (transmembrane activator and calcium-modulator and cyclophilin ligand interactor)] (11). The class switch disorder in IgA-producing B lymphocytes is one of the most important factors in IgAD patients (12). Asano *et al* (13) suggested that the decreased expression level of Iα germline transcripts before a class switch might be the cause of selective IgAD, and that B-cell differentiation might be disturbed after a class switch in partial IgAD patients. Husain *et al* (14) reported that the increased destruction of a subset of B cells is a cause of the inability of IgAD patients to produce IgA. Many studies have reported that certain cytokines, such as IL-4, IL-10, anti-CD40 and TGF-ß, play important roles in the production of IgA (15,16).

The molecular weights of the IgA heavy chain of the α1 and α2 genes are approximately 53 kD each, and the α-chain constant region is encoded by three exons: Cα1, Cα2 and Cα3. Cα2 includes a hinge region at its 5'-end. The hinge region of the α2 gene has a deletion of 13 amino acids compared with that of the α1 gene (1,17). The genes encoding α1 and α2 resemble each other closely and, in IgAD patients in particular, it has been difficult to make a quantitative analysis. In order to elucidate the pathogenesis of, and immunological reaction to, IgAD, we analyzed the gene expression of the IgA subclasses in IgAD patients. In this study, we devised a semiquantitative method in order to determine the gene expression levels of members of the IgA subclasses, and analyzed selective, partial and secondary IgAD patients. Using this method, the gene expression of the IgA subclasses could be analyzed in detail.

Materials and methods

Subjects. As shown in Table I, we analyzed three selective IgAD patients (nos. 1, 2 and 3) with serum IgA levels below the detection limit (<5 mg/dl), five partial IgAD patients (nos. 4, 5, 6, 7 and 8) with serum IgA levels >5 mg/dl but -2 standard deviations below the normal levels, and two

Correspondence to: Dr Hiroko Suzuki, Department of Pediatrics, Graduate School of Medicine, Gifu University, 1-1 Yanagido, Gifu 501-1194, Japan
E-mail: hori_hiro2002@yahoo.co.jp

Key words: immunoglobulin A deficiency, immunoglobulin A subclasses, IgA1/IgA2 gene expression ratios, TGF-ß1

Table I. Immunological data of patients.

Patient no.	Gender	Age (years)	Serum level (mg/dl)			IgG subclass (mg/dl)			
			IgG	IgA	IgM	IgG1	IgG2	IgG3	IgG4
Selective IgA deficiency									
1	M	10	1363	<5	146	619	255.0	57.3	33.9
2	F	11	1640	<5	117	949	400.0	47.7	90.2
3	F	17	1261	<5	137	630	625.0	35.1	18.4
Partial IgA deficiency									
4	M	4	1223	17	120	933	<8.0	22.8	<3.0
5	F	3	1644	15	150	878	47.9	17.3	32.1
6	F	3	869	27	106	306	69.3	27.6	3.8
7	M	4	887	45	101	295	97.0	40.0	4.4
8	M	4	1624	8	100	1090	120.0	74.7	<3.0
Secondary IgA deficiency									
9	F	7	913	12	105	602	148.0	52.8	16.5
10	M	13	705	9	39	852	345.0	49.8	6.4

secondary IgAD patients (nos. 9 and 10) whose condition was caused by epileptic medication. Ten controls were also included in this study. We obtained informed consent from the patients, controls or their parents.

Cell preparation and culture. Peripheral blood mononuclear cells (PBMCs) were collected in heparin and separated by gradient centrifugation in Ficoll-Paque (Amersham Bioscience, Uppsala, Sweden) (18). Cells were suspended at a density of 10^6/ml and cultured for 24 h in an RPMI-1640 medium supplemented with 10% heat-inactivated fetal calf serum, 2 mmol/l L-glutamine, 100 U/ml penicillin and 100 μg/ml streptomycin. Some of the PBMCs were stimulated with phorbol myristate acetate (PMA) (10 ng/ml) (Sigma Aldrich, St. Louis, MO, USA) and recombinant human TGF-ß1 (1 ng/ml) (R&D Systems, Inc., Wiesbaden, Germany) for 24 h.

cDNA synthesis and PCR amplification. We extracted total RNA from PBMCs using an Isogen kit (Nippon Gene, Tokyo, Japan), and cDNA synthesis was carried out using 2 μg of total RNA with oligo-dT and M-MLV reverse transcriptase (Invitrogen, Carlsbad, CA). We used the following PCR primers, both of which were designed against the common sequence area of the α1 and α2 genes: sense 5'-CCT GGT CAC CGT CTC CTC A-3' (within the J exon; Gene Bank accession no. L20778) and antisense 5'-TCA CGC TCA GGT GGT CCT TG-3' (within the Cα CH2 exon) (19). The PCR fragments included the CH1, hinge and CH2 regions, and their sizes were 532 bp for the α1 gene and 493 bp for the α2 gene. The PCR program was 35 or 40 cycles of 94˚C for 1 min, 60˚C for 1 min, and 72˚C for 1 min, using 1 or 2 μl of cDNA as the template. The PCR products were run on 4% agarose gels for 120 min. Glyceraldehyde-3-phosphate dehydrogenase (GAPDH) was used as a control.

Zone densitometry analysis. The IgA1/IgA2 gene expression ratios in stimulated cells were measured using zone densitometry. The peaks of each of the three bands were detected and measured. Half of the intensity of the heterozygous band was added to each of the α1 and α2 band intensities, and then the IgA1/IgA2 ratios were calculated. Subcloning was conducted according to the following steps. After electrophoresis the bands, including the α1 and α2 genes, were cut out, and DNA extraction was performed. We transformed the DNA fragments into a T-vector, then cultured and picked up the colonies. The plasmid DNA was extracted and digested to completion with *Eco*RI. We distinguished two isotypes, α1 and α2 genes, by the sizes of DNA bands on the gels; some of the α2 fragments were separated into two bands because one of the allotypes of the α2 gene, the A2m(2) allotype, had an *Eco*RI site (20).

Quantification of IgA in plasma. IgA was measured using enzyme-linked immunosorbent assay (ELISA). ELISA plates were coated overnight at 4˚C with goat anti-human IgA (Bethyl, Montgomery, TX), which was diluted to 1:100 with 0.05 M sodium carbonate, pH 9.6. After washing, the plates were incubated with standard serum and plasma dilutions. IgA was detected by horseradish peroxidase (HRP)-labeled goat anti-human IgA (Cappel, Organon Teknika, Turnhout, Belgium), which was diluted to 1:10,000 with 1% BSA, 50 mM Tris-HCl, pH 8.0, 0.15 M NaCl and 0.05% Tween-20. The samples were tested repeatedly. The lower limit of IgA detection was 5 ng/ml.

Quantification of IgA subclasses in plasma. The levels of the IgA subclasses in plasma were measured using ELISA. For IgA1, coating was performed using a mouse monoclonal anti-IgA1 antibody (NI69-11), and detection of IgA1 was

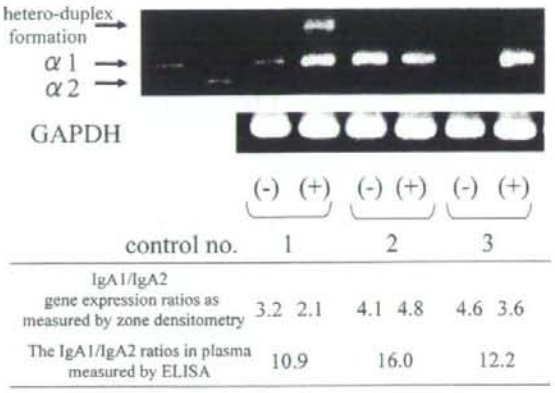

Figure 1. Expression of the α1 and α2 genes in healthy controls. PBMCs from three healthy controls were cultured for 24 h in the absence or presence of stimulation with TGF-ß1 and PMA. After PCR, three bands appeared representing α2 and α1 gene expression and hetero-duplex formation, as indicated by arrows. GAPDH was used as a control. The IgA1/IgA2 expression ratios following stimulation were measured by zone densitometry, and the IgA1/IgA2 ratios in plasma were measured using ELISA.

performed using an HRP-labeled goat anti-human IgA antibody (Cappel, Organon Teknika) (21). For IgA2, coating was performed with goat anti-human IgA, and detection of IgA2 was performed using a mouse anti-human IgA2-HRP antibody (B3506B4) (22). ELISA plates were coated overnight at 4˚C with mouse monoclonal anti-IgA1 (diluted to 1:200 with PBS-0.02% Tween-20) or goat anti-human IgA (diluted to 1:100 with PBS-0.02% Tween-20). After washing, plates were incubated with standard serum and plasma dilutions. IgA1 was detected using goat anti-human IgA-HRP antibody (diluted 1:10,000 with PBS-0.02% Tween-20), and IgA2 was detected using mouse anti-human IgA2-HRP antibody (diluted to 1:1000 with PBS-0.02% Tween-20). Samples were tested repeatedly. The lower limits of IgA1 and IgA2 detection were 5 and 1 μg/ml, respectively.

Statistical analysis. Significant differences between two groups were analyzed by paired t-tests. The correlation coefficients were determined by Pearson's product-moment correlation coefficient. $p<0.05$ was considered to be statistically significant.

Results

PCR amplification of α1 and α2 gene expression in control PBMCs. RT-PCR analysis was performed using primer pairs that amplified both α1 and α2 mRNAs and could distinguish between them owing to the deletion of 39 bases in the hinge region of the α2 mRNA. As shown in Fig. 1, the controls displayed an intense α1 band and a less intense, shorter α2 band in all three PCR conditions. Another band with less electrophoretic mobility than the α1 band was determined to be a hetero-duplex formation from the α1 and α2 fragments, because the subcloning of this band yielded clones of both α1 and α2 fragments. The expression of the α1 and α2 genes in the healthy controls is shown in Fig. 1. The gene expression of the PCR products tended to be enhanced more strongly when cells were stimulated with TGF-ß1 and PMA. In all of the healthy controls, α1 gene expression was dominant. The IgA1/IgA2 expression ratios were measured by zone densitometry in the healthy controls and were found to vary (1.1-4.8) among the controls. There were no significant differences in the IgA1/IgA2 expression ratios of unstimulated cells and cells stimulated with TGF-ß1/PMA ($p>0.05$). To confirm the IgA1/IgA2 ratios as analyzed by zone densitometry, we counted the number of colonies from the PCR products. The

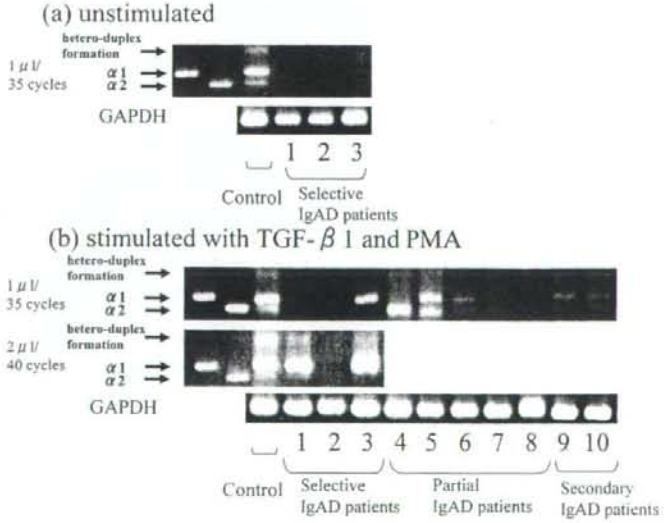

Figure 2. Expression of the α1 and α2 genes in IgAD patients. PBMCs from IgAD patients were cultured for 24 h in the absence (a) or presence (b) of stimulation with TGF-ß1 and PMA. In each case, 1 or 2 μl of cDNA was used as a template and 35 or 40 cycles were run. GAPDH was used as a control.

number of colonies correlated with the IgA1/IgA2 ratios determined by zone densitometry (data not shown).

PCR amplification of α1 and α2 gene expression in IgAD patients. Expression of the α1 and α2 genes in the IgAD patients is shown in Fig. 2. Stimulation of cells with TGF-ß1/PMA induced expression of mature transcripts in some selective IgAD patients. No selective IgAD patients showed any bands without stimulation, while selective IgAD patients (nos. 1 and 3) showed two or three bands following stimulation. Some partial IgAD patients (nos. 5, 6 and 7) and secondary IgAD patients (nos. 9 and 10) showed α2, α1 and heteroduplex gene expression following stimulation, while patient no. 4 showed only α2 gene expression. This patient was found to have a deletion of α1, γ2, γ4 and ε genes, as in a previously reported case (10). Using this method, we identified the second case of α1 gene deletion in Japan. Partial IgAD patient no. 8 showed no bands using this RT-PCR method. The IgA1/IgA2 ratios of IgAD patients analyzed by zone densitometry are shown in Table II. ND (not detected) in Table II means that gene expression was not detected or that the peaks were too faint to detect when analyzed by zone densitometry. The expression levels of both the α1 and α2 genes relative to GAPDH expression in IgAD patients were suppressed when compared with the controls (data not shown). In selective IgAD patients, both α1 and α2 gene expression was induced following stimulation. In particular, α1 gene expression was more dominant than that of α2 in these patients when compared with the other IgAD patients and healthy controls.

IgA, IgA1 and IgA2 concentration in the controls and IgAD patients. The levels of IgA1 and IgA2 proteins in plasma are shown in Table III. ND (not detected) in Table III means that levels were below the detection limit. In all controls, the IgA1 levels in plasma were dominant. The IgA1/IgA2 gene expression ratios following stimulation measured by zone densitometry were strongly correlated with those of plasma levels measured using ELISA in the controls (n=10, r=0.917, t=6.53, p<0.05) (Fig. 1).

Table II. IgA1/IgA2 gene expression ratios measured by zone densitometry.

Patient no.	IgA1/IgA2 gene ratios	
	Stimulation	
	(-)	TGF-ß1/PMA
Selective IgA deficiency		
1	ND	3.91±0.55
2	ND	ND
3	ND	7.04±1.22
Partial IgA deficiency		
4		No α1 gene transcripts
5		2.55±1.74
6		1.72±0.49
7		1.11±0.27
8		ND
Secondary IgA deficiency		
9		1.50±0.29
10		1.17±0.10
Controls (n=10)	2.56±1.22	2.35±1.20

ND, not detected.

Table III. IgA subclass levels and the IgA1/IgA2 ratios in plasma as measured using ELISA.

Patient no.	Plasma IgA, IgA1 and IgA2 levels (mg/dl)			IgA1/IgA2 ratios
	IgA	IgA1	IgA2	
Selective IgA deficiency				
1	2.13±0.01	2.48±0.26	ND	NC
2	ND	ND	ND	NC
3	4.00±0.59	2.16±0.74	ND	NC
Partial IgA deficiency				
4	9.18±2.87	ND	13.7±1.39	NC
5	5.16±0.21	2.71±0.36	ND	NC
6	10.11±0.13	8.28±0.52	0.91±0.25	8.40
7	37.46±8.36	29.29±6.83	4.88±0.54	6.97
8	6.53±0.52	6.28±0.67	0.86±0.45	8.87
Secondary IgA deficiency				
9	11.23±1.91	8.59±1.77	1.17±0.36	6.56
10	0.54±0.06	0.56±0.09	0.18±0.03	3.03
Controls (n=10)	154.01±37.89	119.61±34.69	20.44±8.63	7.96±4.14

ND, not detected; NC, not calculated.

Discussion

The serum IgA subclass levels of IgAD patients, especially selective IgAD patients, are very difficult to measure using ELISA, so there have been few reports concerning them. The expression levels of the α1 and α2 genes in most IgAD patients are low, and there have been no reports concerning the levels of mature transcripts of the IgA subclasses in patients (23-26). Wang *et al* (27) concluded that the cause of IgAD is a defect in the transcriptional factors important for post-switch Cα gene transcription or a lack of signals for activation of the Cα gene in IgA-switched cells. According to Hummelshoj *et al* (16), α1 and α2 germline transcripts in IgAD patients were induced by the stimulation of certain types of cytokines, such as TGF-ß1 and IL-4. Such stimulation can lead to the induction of germline transcripts and mature transcripts in IgAD patients. In our report, using stimulation of cells with TGF-ß1 and PMA, we induced expression of both α1 and α2 transcripts in cells from IgAD patients and measured the IgA1/IgA2 ratios. In the healthy controls, there were no significant differences in the IgA1/IgA2 ratios with or without stimulation. In the IgAD patients, the gene expression levels of both IgA subclasses were suppressed. Expression of the α1 gene was induced more dominantly than that of the α2 gene following stimulation in selective IgAD patients. Kitani and Strober (28) reported that *Staphylococcus aureus*, Cowan I and TGF-ß1 induce mature Cα1 transcripts, but do not induce Cα2 mature transcripts. Based on our results, suppression of α1 gene expression may be involved in the pathogenesis of selective IgAD. However, there was a discrepancy in the IgA1/IgA2 ratios based on gene expression levels and those based on protein expression levels. This discrepancy might have been caused by post-transcriptional modifications leading to, for example, protein or mRNA stability. The other possibility is that the production of IgA protein might have been different in peripheral circulating IgA-switched B cells and locally accumulated IgA-switched B cells, such as mucosal tissue. Secreted and membrane-localized IgA can not be distinguished by this method, and we are now investigating methods for the separation of membrane and secretory transcripts in each IgA subclass.

Our method was effective for detecting mature transcripts of IgA subclasses in cases whose serum IgA levels were under the detection limit. Additional patient analysis is needed to clarify the mechanism of the pathogenesis of IgAD.

Acknowledgements

This study was supported in part by a grant from The Ministry of Health, Labor and Welfare of Japan.

References

1. Kerr MA: The structure and function of human IgA. Biochem J 271: 285-296, 1990.
2. Kazeeva TN and Shevelev AB: Unknown functions of immunoglobulin A. Biochemistry 72: 485-494, 2007.
3. Cunningham-Rundles C: Physiology of IgA and IgA deficiency. J Clin Immunol 21: 303-309, 2001.
4. Hammarstrom L, Vorechovsky I and Webster D: Selective IgA deficiency and common variable immunodeficiency. Clin Exp Immunol 120: 225-231, 2000.
5. Latiff AH and Kerr MA: The clinical significance of immunoglobulin A deficiency. Ann Clin Biochem 44: 131-139, 2007.
6. Schaffer FM, Monteiro RC, Volanakis JE and Cooper MD: IgA deficiency. Immunodefic Rev 3: 15-44, 1991.
7. Bottaro A, De Marchi M, De Lange GG and Carbonara AO: Gene deletions in the human immunoglobulin heavy chain constant region gene cluster. Exp Clin Immunogenet 6: 55-59, 1989.
8. Lefranc MP, Hammarstrom L, Smith CI, *et al*: Gene deletions in the human immunoglobulin heavy chain constant region locus: molecular and immunological analysis. Immunodefic Rev 2: 265-281, 1991.
9. Plebani A, Carbonara AO, Bottaro A, *et al*: Gene deletion as cause of associated deficiency of IgA1, IgG2, IgG4 and IgE. Immunodefic Rev 4: 245-248, 1993.
10. Terada T, Kaneko H, Li AL, Kasahara K, Ibe M, Yokota S and Kondo N: Analysis of Ig subclass deficiency: first reported case of IgG2, IgG4, and IgA deficiency caused by deletion of Cα1, ψCγ, Cγ2, Cγ4 and Cε in a Mongoloid patient. J Allergy Clin Immunol 108: 602-606, 2001.
11. Castigli E, Wilson SA, Garibyan L, Rachid R, Bonilla F, Schneider L and Geha RS: TACI is mutant in common variable immunodeficiency and IgA deficiency. Nat Genet 37: 829-834, 2005.
12. Islam KB, Baskin B, Nilsson L, Hammarstrom L, Sideras P and Smith CI: Molecular analysis of IgA deficiency. J Immunol 152: 1442-1452, 1994.
13. Asano T, Kaneko H, Terada T, Kasahara Y, Fukao T, Kasahara K and Kondo N: Molecular analysis of B-cell differentiation in selective or partial IgA deficiency. Clin Exp Immunol 136: 284-290, 2004.
14. Husain Z, Holodick N, Day C, Szymanski I and Alper CA: Increased apoptosis of $CD20^+IgA^+B$ cells is the basis for IgA deficiency: The molecular mechanism for correction *in vivo* by IL-10 and CD40L. J Clin Immunol 26: 113-125, 2006.
15. Marconi M, Plebani A, Avanzini MA, *et al*: IL-10 and IL-4 cooperate to normalize *in vivo* IgA production in IgA-deficient patients. Clin Exp Immunol 112: 528-532, 1998.
16. Hummelshoj L, Ryder LP, Nielsen LK, Nielsen CH and Poulsen LK: Class switch recombination in selective IgA-deficient subjects. Clin Exp Immunol 144: 458-466, 2006.
17. Koteswara R: Divergence of human α-chain constant region gene sequences. J Immunol 152: 5299-5304, 1994.
18. Kondo N, Fukutomi O, Agata H, *et al*: The role of T lymphocytes in patients with food-sensitive atopic dermatitis. J Allergy Clin Immunol 91: 658-668, 1993.
19. Klasen IS, Goertz JHC, van de Wiel GA, Weemaes CM, van der Meer JW and Drenth JP: Hyper-Immunoglobulin A in the hyper-immunoglobulinemia D syndrome. Clin Diagn Lab Immunol 8: 58-61, 2001.
20. Lefranc MP and Rabbits TH: Human immunoglobulin heavy chain A2 gene allotype determination by restriction fragment length polymorphism. Nucleic Acids Res 12: 1303-1311, 1984.
21. Camacho MT, Outschoorn I, Echevarria C, *et al*: Distribution of IgA subclass response to *Coxiella burnetii* in patients with acute and chronic Q fever. Clin Immunol Immunopathol 88: 80-83, 1998.
22. Beard LJ and Ferrante A: IgG4 deficiency in IgA-deficient patients. Pediatr Infect Dis J 8: 705-709, 1989.
23. Vlasselaer PV, Punnonen J and Vries JE: Transforming growth factor-ß directs IgA switching in human B cells. J Immunol 148: 2062-2067, 1992.
24. Park SR, Kim HA, Chun SK, Park JB and Kim PH: Mechanisms underlying the effects of LPS and activation-induced cytidine deaminase on IgA isotype expression. Mol Cells 19: 445-451, 2005.
25. Islam KB, Nilsson L, Sideras P, Hammarstrom L and Smith CI: TGF beta-1 induces germ-line transcripts of both IgA subclasses in human B lymphocyte. Int Immunol 3: 1099-1106, 1991.
26. Nilsson L, Islam KB, Olafsson O, *et al*: Structure of TGF-beta 1-induced human immunoglobin C alpha 1 and alpha 2 germ-line transcripts. Int Immunol 3: 1107-1115, 1991.
27. Wang Z, Yunis D, Irigoyen M, Kitchens B, Bottaro A, Alt FW and Alper CA: Discordance between IgA expression and the mRNA level in IgA-deficient patients. Clin Immunol 91: 263-270, 1999.
28. Kitani A and Strober W: Differential regulation of Cα1 and Cα2 germ-line and mature mRNA transcripts in human peripheral blood B cells. J Immunol 153: 1466-1477, 1994.

Available online at www.sciencedirect.com
ScienceDirect
Transfusion and Apheresis Science 38 (2008) 199–201
TRANSFUSION AND APHERESIS SCIENCE
intl.elsevierhealth.com/journals/tras

Brief report

Anaphylactoid transfusion reactions associated with a positively charged white-cell reduction filter: A case report

Michinori Funato *, Hideo Kaneko, Michio Ozeki, Kaori Kanda, Toshiyuki Fukao, Naomi Kondo

Department of Pediatrics, Gifu University Graduate School of Medicine, Yanagido 1-1, Gifu 501-1194, Japan

Abstract

The effectiveness of a white-cell reduction filter to deplete contaminated leucocytes in preventing the harmful effects of transfusion is evident. However, several complications associated with a white-cell reduction filter have been identified. We report the first case of anaphylactoid reactions caused by a white-cell reduction filter with a positively charged surface.

1. Introduction

In 1990 Tielemans et al. described a life-threatening anaphylactoid reaction occurring within the very first minutes of hemodialysis using polyacrylonitrile (AN69) capillary dialyzers in three patients receiving angiotensin-converting enzyme (ACE) inhibitors [1]. In 1992 Olbricht et al. also described a similar anaphylactoid reaction due to low-density lipoprotein (LDL)-apheresis with dextran sulphate adsorption in patients receiving ACE inhibitors [2]. These anaphylactoid reactions were thought to be due to a bradykinin formation cascade, activated by using negatively charged white-cell reduction filters [3]. So far, several anaphylactoid reactions associated with white-cell reduction filters have been reported. However, anaphylactoid reactions associated with white-cell reduction filters having a positively charged surface have not been reported previously. Herein, we describe the first case of anaphylactoid reactions caused by a white-cell reduction filter with a positively charged surface in this paper.

2. Case report

A boy with recurrent anaplastic ependymoma of the brain was on chemotherapy at seven years of age. He had a pollen allergy. His father was Japanese and his mother was Filipino. At three years of age, he was found to have a brain tumor and received a complete surgical resection. At that time, he was not given a blood transfusion. Four years later, brain computed tomography (CT) showed a 6×5 cm mass lesion in the left frontal horn, which meant a recurrence of anaplastic ependymoma. He was subsequently treated by a total excision of the tumor. Postoperatively, he received radiation

* Corresponding author. Tel.: +81 58 2306386; fax: +81 58 2306387.
E-mail address: mfunato@mac.com (M. Funato).

1473-0502/$ - see front matter © 2008 Elsevier Ltd. All rights reserved.
doi:10.1016/j.transci.2008.03.006

therapy (a total of 30 Gy), stereotactic radiosurgery (SRS) (a total of 12 Gy) and four courses of multi-agent chemotherapy consisting of vincristine, etoposide, cyclophosphamide and cisplatin.

He required some transfusions of red blood cells, platelets and fresh frozen plasma for the side effects of bone marrow suppression during the treatment (Table 1). There was no trouble during the first and second transfusions of packed red blood cells and fresh frozen plasma, respectively. However, after starting infusion of leukocyte-poor red cells, which were filtered with a positively charged white-cell reduction filter (Sepacell RZ-2 filter, Asahi Med, Japan), as a third transfusion, he immediately developed a skin rash of the trunk, hypotension, blurred eyesight and unconsciousness. No stridor or dyspnea was observed. The transfusion was stopped and he was rescued by fluid resuscitation, epinephrine and hydrocortisone. We thought his reaction was allergic, associated with the transfusion. In the next infusion, washed red blood cells were used and nothing happened. In the fifth transfusion, we gave him prophylactic antihistamines and infused leukocyte-poor red cells, and similar anaphylactoid symptoms occurred immediately. His symptoms were resolved in several minutes by medical treatment. Subsequent transfusions of washed red blood cells or a platelet concentration were done without any problem.

3. Discussion

A transfusion of allogeneic cellular blood products is associated occasionally with adverse reactions and other complications, including febrile nonhemolytic transfusion reactions (FNHTR), graft-versus-host disease (GVHD), and immunomodulation and transmission of infectious agents, despite careful donor selection and extensive testing [4]. The use of a white-cell reduction filter to deplete contaminated leucocytes is effective in reducing those harmful effects of transfusion, particularly alloimmunization and cytomegalovirus infection [5]. However, several complications associated with a white-cell reduction filter have been described. Herein, we have reported a rare case of anaphylactoid reactions associated with a white-cell reduction filter having a positively charged surface in a 7-year-old boy.

We thought his symptoms were caused by something related to the positive charge on the membrane. The leukocyte-poor red cells were made from washed red blood cells by passing them through a positively charged white-cell reduction filter at The Japan Red Cross. This patient only developed anaphylactoid symptoms twice when the former but not the latter was transfused. In addition, his clinical symptoms were very similar to anaphylactoid reactions during transfusion associated with a negatively charged white-cell reduction filter, which was reported in previous literature [6]. The possibility of other causes is unlikely, because his antibodies against HLA, IgA, haptoglobin, C4, C9, ceruloplasmin, and anti-alpha-2-microglobulin were all negative when examined at The Japan Red Cross Central Blood Center. In addition, this patient had a mild increase in his peripheral eosinophil count (0.603×10^9/L) for allergic constitution and normal immunoglobulin G, A, M and E concentrations (1149 mg/dl, 175 mg/dl, 178 mg/dl and 150 IU/L, respectively).

Iwama examined the effect of temperature on bradykinin generation during the use of white-cell reduction filters. In this assay, a positively charged filter did not generate bradykinin at any temperature. However, a negatively charged one generated a lot of bradykinin when warm blood (37 °C) was

Table 1
All courses of transfusion in this patient during the treatment

No.	Blood product	Anaphylactoid reaction	A positively white-cell reduction filter	Prophylactic agent
1	Packed red blood cells	−	−	−
2	Fresh frozen plasma	−	−	−
3	Leukocyte-poor red cells	+	+	−
4	Washed red blood cells	−	−	−
5	Leukocyte-poor red cells	+	+	+
6	Platelet concentration	−	−	+
7	Washed red blood cells	−	−	+
8	Washed red blood cells	−	−	+
9	Washed red blood cells	−	−	+
10	Platelet concentration	−	−	+
11	Washed red blood cells	−	−	+

used but did not when cool blood (4 °C) was used [7]. In our patient, The Japan Red Cross prepared leukocyte-poor red cells at 4 °C and kept them at 4 °C. Then a blood transfusion was done at room temperature. Hence, bradykinin was not likely to cause any symptoms in our patient.

This case of anaphylactoid transfusion reactions associated with a positively charged white-cell reduction filter may be attributed to the fact that such reactions are not related to the charge on the membrane, but to a hypersensitivity reaction against something made by filtration through a white-cell reduction filter. In this respect, further work needs to be undertaken on the exact molecular nature of this reaction.

Acknowledgements

This study was supported in part by the Health and Labor Science Research Grants of the Research on Allergic disease and Immunology from the Ministry of Health, Labor and Welfare.

References

[1] Tielemans C, Madhoun P, Lenaers M, Schandene L, Goldman M, Vanherweghem JL. Anaphylactoid reactions during hemodialysis on AN69 membranes in patients receiving ACE inhibitors. Kidney Int 1990;38:982–4.

[2] Olbricht CJ, Schaumann D, Fischer D. Anaphylactoid reactions, LDL apheresis with dextran sulphate, and ACE inhibitors. Lancet 1992;340:908–9.

[3] Takahashi TA, Abe H, Hosoda M, Nakai K, Sekiguchi S. Bradykinin generation during filtration of platelet concentrates with a white cell-reduction filter. Transfusion 1995;35:967.

[4] Bordin JO, Heddle NM, Blajchman MA. Biologic effects of leukocytes present in transfused cellular blood products. Blood 1994;84:1703–21.

[5] de Graan-Hentzen YCE, Gratama JW, Mudde GC, Verdonck LF, Houbiers JGA, Brand A, et al. Prevention of primary cytomegalovirus infection in patients with hematologic malignancies by intensive white cell depletion of blood products. Transfusion 1989;29:757–60.

[6] Sano H, Koga Y, Hamasaki K, Furuyama H, Itami N. Anaphylaxis associated with white-cell reduction filter. Lancet 1996;347:1053.

[7] Iwama H. Bradykinin-associated reactions in white cell-reduction filter. J Crit Care 2001;16:74–81.

Positioning of autoimmune TCR-Ob.2F3 and TCR-Ob.3D1 on the MBP85–99/HLA-DR2 complex

Zenichiro Kato[†‡§¶‖], Joel N. H. Stern[†], Hironori K. Nakamura[§], Kazuo Kuwata[§], Naomi Kondo[†§¶], and Jack L. Strominger[†]

[†]Department of Molecular and Cellular Biology, Harvard University, Cambridge, MA 02138; and [‡]Department of Pediatrics, Graduate School of Medicine, [§]Center for Emerging Infectious Diseases, and [¶]Center for Advanced Drug Research, Gifu University, 1-1 Yanagido, Gifu 5010-1194, Japan

Contributed by Jack L. Strominger, August 11, 2008 (sent for review July 8, 2008)

Since the first determination of structure of the HLA-A2 complex, >200 MHC/peptide structures have been recorded, whereas the available T cell receptor (TCR)/peptide/MHC complex structures now are <20. Among these structures, only six are TCR/peptide/MHC Class II (MHCII) structures. The most recent of these structures, obtained by using TCR-Ob.1A12 from a multiple sclerosis patient and the MBP85–99/HLA-DR2 complex, was very unusual in that the TCR was located near the N-terminal end of the peptide-binding cleft of the MHCII protein and had an orthogonal angle on the peptide/MHC complex. The unusual structure suggested the possibility of a disturbance of its signaling capability that could be related to autoimmunity. Here, homology modeling and a new simulation method developed for TCR/peptide/MHC docking have been used to examine the positioning of the complex of two additional TCRs obtained from the same patient (TCR-Ob.2F3 or TCR-Ob.3D1 with MBP85–99/HLA-DR2). The structures obtained by this simulation are compatible with available data on peptide specificity of the TCR epitope. All three TCRs from patient Ob including that from the previously determined crystal structure show a counterclockwise rotation. Two of them are located near the N terminus of the peptide-binding cleft, whereas the third is near the center. These data are compatible with the hypothesis that the rotation of the TCRs may alter the downstream signaling.

human leukocyte antigen | multiple sclerosis | myelin basic protein | structural docking | signaling

The elucidation of structures of protein complexes is an arduous procedure particularly when the complexes are very large. The production of protein by recombinant techniques and subsequent crystallization of the complexes followed by x-ray diffraction analysis is a standard method. Structures can also be determined by NMR but that technique is presently limited to only relatively small proteins or complexes not >40–50 kDa. The third method, simulation of structures by homology modeling, has improved greatly in recent years. However, this technique is usable only when an appropriate template structure is available.

Crystallization and structure determination by x-ray diffraction of a MHC-encoded Class I (MHCI) protein/peptide complex was first accomplished in 1987 and MHCII in 1993 (1, 2). Since then, >200 structures of such complexes have been recorded (3). The β chain of the TCRs that recognize these complexes were first cloned in 1984 (4, 5), and the first structure of a TCR chain was published in 1995 (6). Approximately 40 complete TCR structures including both α and β chains are available now (3, 7). Similarly, the first TCR/peptide/MHC complex structures were published in 1996 (8, 9) but the number of such complex structures available now is <20 (3). Among these, only six are TCR/peptide/MHCII structures. The most recent of these structures is very unusual in that the TCR was located near the N-terminal end of the peptide-binding cleft of the MHCII protein and its orthogonal angle on the MHCII/peptide was 84° as compared with a diagonal angle of 40–53° for the other five structures (10). Also, it was rotated counterclockwise on the MHC molecule relative to the other structures. This unusual structure suggested the possibility of a disturbance of its signaling capability that could be related to autoimmunity because this TCR, termed Ob.1A12 had been obtained from an autoreactive clone derived from a patient with multiple sclerosis (10). In fact, eight clones were obtained from this patient, two of which represent unique isolates (TCR-Ob.1A12 and TCR-Ob.3D1) and six of which have identical sequences, TCR-Ob.2F3 being an example (11).

In this article, we have used homology modeling of TCR structures on the appropriate templates and a new simulation method developed for TCR/peptide/MHC docking to examine the structures of the TCR/peptide/MHCII complexes of TCR-Ob.2F3 and TCR-Ob.3D1 in complex with the same MHC/peptide, namely HLA-DR2 (DRB1*1501/DRA) binding the myelin basic protein peptide epitope MBP85–99. MBP85–99 has previously been identified as the autoreactive peptide epitope in humans (12).

Results and Discussion

The AutoDock procedure was originally developed for docking studies of small chemicals to their receptors, for example the docking of a substrate to an enzyme (13). It makes use of charge and hydrophobicity calculations for both the receptor and the ligand (see *Materials and Methods*). By using this method in the present context, the peptide in question was first docked to the appropriate MHC molecule and separately to the TCR protein. The conformation of the peptide used in the docking in each case was taken from the crystal structure of the MBP85–99/HLA-DR2 (DRB1*1501, DRA) complex (10). After TCR/peptide and peptide/MHC structures were simulated, the two structures were merged by using the conformation of the peptide as the basis for merging. To validate the procedure, the technique was carried out by using two known TCR/peptide/MHC structures, that of the HLA-DR1 (DRB1*0101/DRA)/hemagglutinin (HA) 306–318 molecule in complex with the HLA-DR1-restricted HA306–318-specific TCR-HA1.7 (PDB ID code 1FYT) and then of the HLA-DR2/MBP85–99 molecule in complex with TCR-Ob.1A12 (PDB ID code 1YMM).

Simulated Structure of the TCR-HA1.7/HA306–318/HLA-DR1 Complex and the TCR-Ob.1A12/MBP85–99/HLA-DR2 Complex. The docking of HA306–318 to HLA-DR1 was simulated 10 times. Six of the 10 simulations showed exactly the same conformation inside the peptide-binding groove with energy equal to −33.8 kcal/mol (Fig. 1*A*). Four of the 10 showed different conformations binding outside of the groove with higher energies of −5.59, −5.59,

Author contributions: Z.K., J.N.H.S., K.K., N.K., and J.L.S. designed research; Z.K. and H.K.N. performed research; Z.K. and H.K.N. analyzed data; and Z.K., J.N.H.S., and J.L.S. wrote the paper.

The authors declare no conflict of interest.

To whom correspondence may be addressed. E-mail: zenkato@mac.com or jlstrom@fas.harvard.edu.

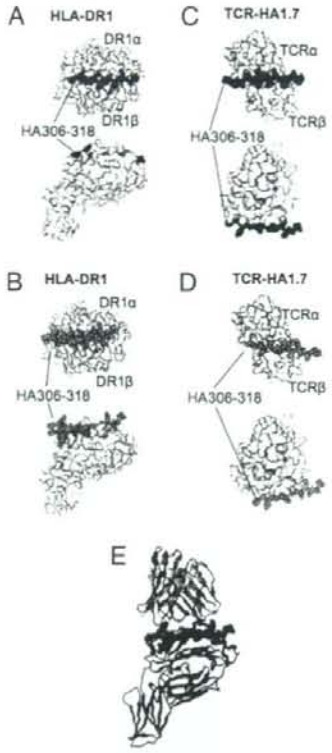

Fig. 1. Docking simulation of the HA306–318 peptide on HLA-DR1 and on TCR-HA1.7. (*A*) The six clustered docked peptides of HA306–318 on HLA-DR1 are indicated as space filling models in brown. (*B*) The four nonclustered docked peptides are indicated as space filling models in yellow. In *A* and *B*, HLA-DR1 (DRB1*0101/DRA) (20) is shown as a surface model in white. (*C*) The nine clustered docked peptides of HA306–318 on TCR-HA1.7 are indicated as space filling models in brown. (*D*) The one nonclustered docked peptide is shown as a space-filling model in yellow. In C and *D*, TCR-HA1.7 is shown as a surface model in white. (*E*) Merging of the docked TCR-HA1.7/HA306–318 and HA306–318/HLA-DR1 was carried out by using the conformation of the peptide as the basis for merging. Superposition was performed between the docked structure and the crystal structure of TCR-HA1.7/HA306–318/HLA-DR1 (20). Docked structure of TCR-HA1.7 in cyan, HA306–318 in brown, and crystal structures of both TCR-HA1.7 and HLA-DR1 in blue. The two TCR structures were superimposed by means of structures of HA306–318.

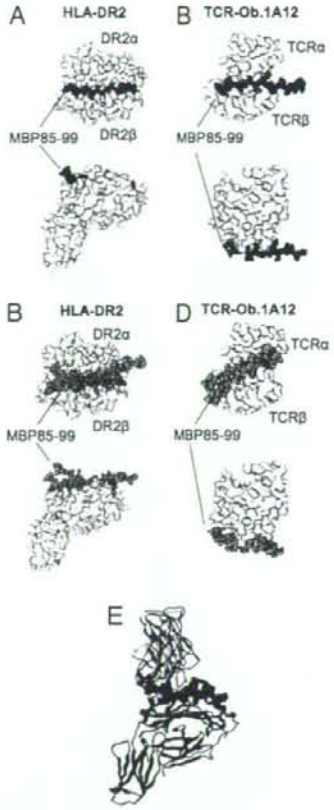

Fig. 2. Docking simulation of the MBP85–99 peptide on HLA-DR2 and on TCR-Ob.1A12. (*A*) The four clustered docked peptides of MBP85–99 on HLA-DR2 are indicated as space filling models in brown. (*B*) The six nonclustered docked peptides are indicated as space filling models in yellow. In *A* and *B*, HLA-DR2 (DRB1*1501/DRA) (10) is shown as a surface model in white. (*C*) The six clustered docked peptides of MBP85–99 on TCR-Ob.1A12 are indicated as space filling models in brown. (*D*) The four nonclustered docked peptides are indicated as space filling models in yellow. In C and *D*, TCR-Ob.1A12 is shown as a surface model in white. (*E*) Merging of the docked TCR-Ob.1A12/MBP85–99 and MBP85–99/HLA-DR2 was carried out by using the conformation of the peptide as the basis for merging. Superposition was performed between the docked structure and the crystal structure of TCR-Ob.1A12/MBP85–99/HLA-DR2 (10). Docked structure of TCR-Ob.1A12 in cyan, MBP85–99 in brown, and crystal structures of both TCR-Ob.1A12 and HLA-DR2 in blue. The two TCR structures were superimposed by means of structures of MBP85–99.

−5.68 and −8.73 kcal/mol (Fig. 1*B*). One of the clustered conformations inside the groove with the lowest energy was selected as representative.

Similarly, HA306–318 docking to TCR-HA1.7 was simulated 10 times. Nine of the 10 simulations had almost the same conformation with energy equal to −5.59 kcal/mol five times and energy −5.67 four times (Fig. 1*C*). One of the 10 simulations yielded a different conformation with a higher energy of −5.02 kcal/mol (Fig. 1*D*). Again, one of the five clustered conformations with the lowest energy was selected as representative.

Next, the TCR-HA1.7/HA306–318 simulated complex was merged with the HA306–318/HLA-DR1 simulated complex to give the TCR-HA1.7/HA306–318/HLA-DR1 complex by using the structure of the peptide as the basis for merging (a related procedure was used in a docking study of the dimeric maltose-binding complex involving maltose-binding protein and aspartate receptor, although in this case the octapeptide used was from a functional region of the maltose-binding protein) (14).

This simulated structure of the ternary complex was merged with the structure determined by crystallization and x-ray diffraction and gave excellent reproducibility with a rmsd of 1.64 Å (Fig. 1E). The same procedure was carried out to obtain the TCR-Ob.1A12/MBP85–99/HLA-DR2 structure. The docking of MBP85–99 to HLA-DR2 was simulated 10 times. Four of the 10 simulations showed exactly the same conformations inside the peptide-binding groove with energy equal to −26.8 kcal/mol (Fig. 2*A*). Six of the 10 showed binding outside of the groove each with a different conformation and with much higher energies of −3.02, −4.95, −4.95, −5.54, −5.64 and −5.91 kcal/mol (Fig. 2*B*). One of the clustered conformations inside the groove with the lowest energy was selected as representative.

Fig. 3. Sequence alignment of TCR-Ob.2F3 and TCR-Ob.3D1 with TCR-Ob.1A12. (*A*) Sequence alignment between TCR-Ob.2F3 and TCR-Ob.1A12. (*B*) Sequence alignment between TCR-Ob.3D1 and TCR-Ob.1A12. Differences in amino acids between the two clones are indicated in yellow. *, identical amino acids; +, similar amino acids.

Similarly, MBP85–99 docking to TCR-Ob.1A12 was simulated 10 times. Six of the 10 simulations had almost the same conformation with energy equal to −4.78 five times and energy −4.65 once (Fig. 2*C*). Four of the 10 simulations each yielded a different conformation with a similar energy of −4.50, −5.08, −5.32, and −5.32 kcal/mol (Fig. 2*D*). Again, one of the six clustered conformations with the lowest energy was selected as representative.

The TCR-Ob.1A12/MBP85–99 simulated complex was also merged with the MBP85–99/HLA-DR2 simulated complex as described above to give the TCR-Ob1A12/MBP85–99/HLA-DR2 complex. Merging of the simulated structure with the structure determined by x-ray crystallography gave excellent reproducibility with a rmsd of 1.54 Å (Fig. 2*E*). Thus, by using two known TCR/peptide/MHC complexes, these data provided a validation for the docking procedure used.

Notably, the energies of docking of the two peptides to their respective MHC proteins (−34 and −27 kcal/mol) were much lower than the energies of their docking to their respective TCR (−5.6

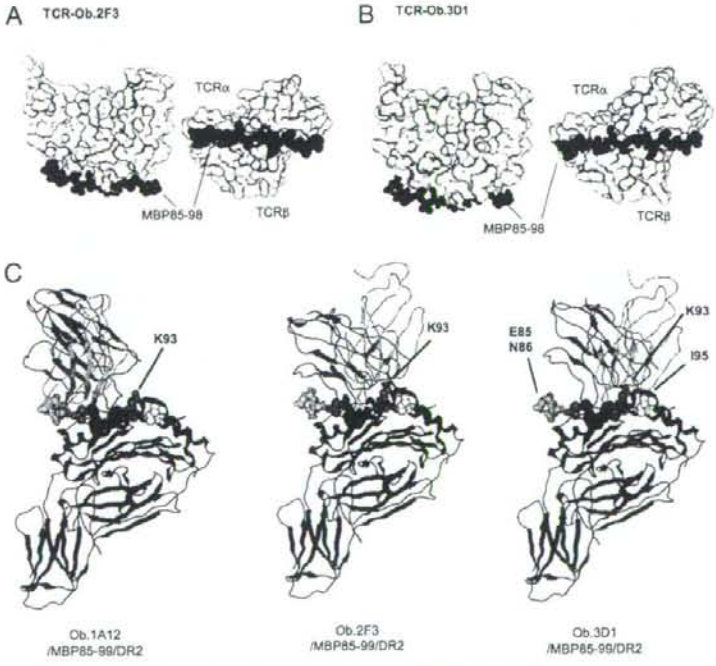

Fig. 4. Positioning of TCR-Ob.2F3 and TCR-Ob.3D1 on MBP85–99/HLA-DR2. (*A*) Docking simulation of the MBP85–99 peptide on TCR-Ob.2F3. The 10 clustered docked peptides are indicated as space filling models in brown. TCR-Ob.2F3 is shown as a surface model in white. (*B*) Docking simulation of the MBP85–99 peptide on TCR-Ob.3D1. The 10 clustered docked peptides are indicated as space filling models in brown. TCR-Ob.3D1 is shown as a surface model in white. (*C*) Comparison of positioning of the TCRs obtained from patient Ob. on the MBP85–99/HLA-DR2 structure. The structures of TCRs, MBP85–99 and HLA-DR2 (DRB1*1501/DRA) are shown as ribbon models. MBP85–99 and HLA-DR2 in blue, the α chains of the three TCRs in yellow, and the β chains of the three TCRs in red. Functionally important residues of MBP85–99 are shown as space filling models, E85 and N86 in green, V88 and K93 in orange, H90 and F91 in red, and I95 in yellow (see *Results and Discussion*).

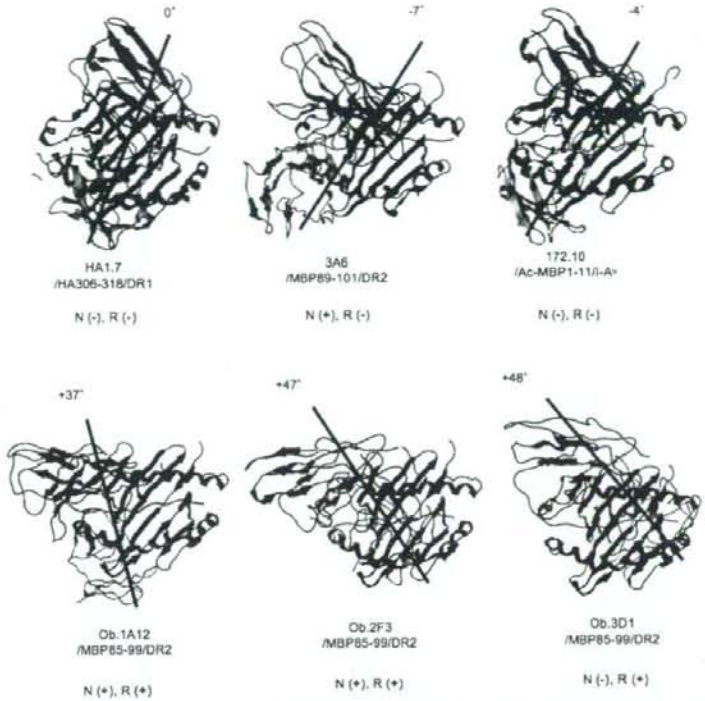

Fig. 5. Comparison of positioning between autoimmune TCRs and nonautoimmune TCR. HA1.7/HA306–318/DR1 indicates the positioning of a nonautoimmune TCR. All of the others are autoimmune TCRs. Black lines are drawn between the S–S bonds of TCRα and TCRβ. Coloring is the same as in Fig. 4C. N, N-terminal shift; R, counterclockwise rotation. The degrees of rotation taking TCR-HA1.7 on HA306–318/HLA-DR1 as 0° were as follows: TCR-3A6, −7°; TCR-172.10, −4°; TCR-Ob.1A12, +37°; Ob.2F3, +47°; and TCR-Ob.3D1, +48°.

and −4.8 kcal/mol). Thus, the binding of the peptide to the MHC proteins is much stronger than the binding to the TCR (13).

Simulated Structure of the TCR-Ob.2F3/MBP85–99/HLA-DR2 Complex and the TCR-Ob.3D1/MBP85–99/HLA-DR2 Complex. Next, structures of two TCR complexes from patient Ob whose complexes with HLA-DR2/MBP85–99 had not been determined were modeled. The sequence alignment with the template TCR-Ob.1A12 of these two TCRs, TCR-Ob.2F3 and TCR-Ob.3D1, are shown in Fig. 3. Notably, TCR-Ob.2F3 has 99% sequence identify with TCR-Ob.1A12 differing at only three amino acid positions. One of these is near the CDR3 loop of the TCR α chain and the other two are in the CDR3 loop of the TCR β chain. By contrast, TCR-Ob.3D1 had only 89% identify in the TCR α chain differing from TCR-Ob.1A12 by 10 positions including two gaps. It had only 37% identify (but 59% similarity) in the β chain differing from the template structure by 40 aa including two insertions in the CDR3 loop.

When MBP85–99 was docked to the modeled TCR-Ob.2F3, the 10 simulations showed almost the same conformation with energies of −5.77 kcal/mol five times, −5.76 four times, and −5.75 once (Fig. 4*A*). One of the clustered confirmations with the lowest energy was again selected as representative. The TCR-Ob.2F3/MBP85–99 docked structure was merged with the crystal structure of MBP85–99/HLA-DR2 again by using the conformation of the MBP85–99 peptide as the basis for merging.

Similarly, MBP85–99 was docked to the model TCR-Ob.3D1 10 times. All 10 simulations showed exactly the same conformation with energy −8.2 kcal/mol (Fig. 4*B*). One of these clustered conformations was again selected as representative and as before docked with the MBP85–99/HLA-DR2 structure.

The structural models that resulted form these simulations are shown in Fig. 4*C*. Several features are obvious. First, like TCR-Ob.1A12 (10), TCR-Ob.2F3 is positioned toward the N-terminus of the peptide-binding groove. However, it is located very slightly more toward the C-terminal end of the peptide. With regard to rotation, the counterclockwise rotation of Ob.1A12 (+37°) as compared with HA1.7 (taken as 0°) is apparent (Fig. 5). The TCR-Ob.2F3 had an even greater counterclockwise rotation (+47°).

TCR-Ob.3D1 by contrast was located near the middle of the peptide-binding cleft at the apex of the helixes in a similar position to TCR-HA1.7 (Figs. 4*C* and 5). However, again its counterclockwise rotation with regard to TCR-HA1.7 was large (+48°) and similar to that of TCR-Ob.2F3. When viewed from the top, the orthogonal angle of all three TCRs was distinct from that of HA1.7 and the other TCR/peptide/MHC complexes whose structures had been determined (5, 3, 15, 16). All three autoimmune TCRs show a counterclockwise rotation and two of them are located near the N-terminus of the peptide-binding cleft. These data are compatible with the hypothesis (10) that the rotation of the TCRs may alter the downstream signaling.

Available data on peptide specificity of the TCR epitope are compatible with these structures (Table 1, compiled from refs. 11, 12, 17, 18). With regard to the peptide, both TCR-Ob.1A12 and TCR-Ob.2F3 are sensitive to deletion of the N-terminal residue 85 of MBP85–99, whereas TCR-Ob.3D1 can recognize even a truncation of two residues at the N-terminus of

Table 1. Characters of the T cell clones from patient Ob

Clone	Ob.1A12	Ob.2F3 Ob.1C3 Ob.1E10 Ob.1E12 Ob.1H8 Ob.2G9	Ob.3D1
Minimal peptide	MBP 85–98	MBP 85–98	MBP 87–98
MBP 85–99	++++	++++	++++
MBP 85–98	++++	++++	++++
MBP 86–98	–	–	++++
MBP 87–98	–	–	++++
MBP 87–97	–	–	–
TCR epitope			
Major	HF—	HF-K–	HF-K–
Minor	—K–	—I	
MBP 85–99	++++	++++	++++
Val88Ala	++++	++++	ND
His90Ala	+	–	–
Phe91Ala	–	–	–
Lys93Ala	++++	++	–
Asn94Ala	++++	+++	+
Ile95Ala	++++	+++	++
Val96Ala	++++	++++	++++

Plus symbol indicates the proliferation of the T cell clones. ND, Not determined. These data are derived from Wucherpfennig *et al.* (11), Wucherpfennig *et al.* (12), Hausmann *et al.* (17), and Wucherpfennig *et al.* (18).

MBP85–99 (Figs. 4C and 5). Alanine scanning of MBP85–99 revealed that TCR recognition of His-90 and Phe-91 was essential for all three clones (Table 1). Only TCR-Ob.3D1 was sensitive to mutation of Asn-94 (P6) or partially Ile-95 (P7), however, K93 was not essential for TCR-Ob.1A12, and K93A revealed reduced sensitivity at this residue for TCR-Ob.2F3 (Table 1). However, both K93A and N94A eliminated reactivity with TCR-Ob.3D1 and I95A reduced reactivity. These data are compatible with the positions of the three TCR as shown in Figs. 4C and 5. Thus, good structure-function correlations are observed in the three autoimmune T cell clones.

The CD4 coreceptor binds to the membrane-proximal MHCII domains and is essential for T cell development and T cell function by recruiting the tyrosine kinase Lck. The alignment of the TCRs observed here showed that the geometry of the interaction with the CD4 coreceptor is altered for the TCRs as previously suggested (10). These findings raise the possibility that CD4 function is affected in immature T cells by an altered geometry of TCR binding to peptide-MHC during the formation of immunological synapses (10). These structures may add to our understanding of the molecular mechanism that could relate to autoimmunity.

Materials and Methods

Structure Modeling of TCR. Structural modeling of TCR-Ob.2F3 and TCR-Ob.3D1 was performed by using MOE software (Chemical Computing Group, www.chemcomp.com) combined with the segment-matching procedure (19, 20). Briefly, the structure of TCR-Ob.1A12 complexed with MBP85–99/HLA-DR2 (10) (PDB ID code 1YMM) was used as a template for homology modeling of TCR-Ob.2F3 and TCR-Ob.3D1. The modeled structure was further energy minimized (MOE software).

Docking Studies of the TCR with Peptide/MHC. Docking was performed by using the AutoDock software package running on Intel-based Xeon, ppcDarwin platform (13). The structure of HLA-DR1 (DRB1*0101/DRA), HLA-DR2 (DRB1*1501/DRA), TCR-HA1.7, TCR-Ob.1A12, TCR-Ob.2F3, or TCR-Ob.3D1 was used as the target structure. HA306–318 or MBP85–99 in the conformation found in their crystal structures (10, 21) was used as the ligand structure. AutoDock with a Lamarckian genetic search algorithm (LGA) was chosen for all dockings (13).

The optimized AutoDocking run parameters were similar to those described in ref. 13 with minor modification in grid size, a maximum number of energy evaluations, and a maximum number of generations. The proteins and ligands in the dockings were treated by using the united-atom approximation. Only polar hydrogens were added to the protein, and Kollman united-atom partial charges were assigned. All waters were removed. Atomic solvation parameters and fragmental volumes were assigned to the protein atoms by using an AUTODOCK utility, ADDSOL and the grid maps were calculated by using AUTOGRID (13).

The dimensions of the grids for docking were thus $180 \times 80 \times 90$ points (67.5 Å $\times$ 30.0 Å $\times$ 33.7 Å) and a grid-point spacing of 0.375 Å, and the center of the grids were placed to cover the surface of the HLA or TCR structure. The ligand was treated initially as all atom entities, i.e., all hydrogens were added, then partial atomic charges were calculated by using the Gasteiger-Marsili method (13). AUTOTORS, an AUTODOCK utility, was used to define the rotable bonds in the ligand to unite the nonpolar hydrogens added by SYBYL for the partial atomic charge calculation. The partial charges on the nonpolar hydrogens were added to that of the hydrogen-bearing carbon also in AUTOTORs.

In the analyses, 10 dockings were performed; in the analysis of the docked conformations, the clustering tolerance as different conformations for the rmsd was 1.0 Å. The step sizes were 0.2 Å for translations and 5° for orientations and torsions. The α and β parameters determined the size of the mutation in the genetic algorithms, LGA. The Cauchy distribution parameters were: $\alpha = 0$ and $\beta = 1$. Note that random changes were generated in the genetic algorithm by a Cauchy distribution.

In the LGA dockings, an initial population of random individuals with a population size of 50 individuals was used; a maximum number of 2.5×10^6 energy evaluations; a maximum number of generations of 2.7×10^4; an elitism value of 1, which was the number of top individuals that automatically survived into the next generation; a mutation rate of 0.02, which was the probability that a gene would undergo a random change; and a cross-over rate of 0.80, which was the probability that two individuals would undergo cross-over. Proportional selection was used, where the average of the worst energy was calculated over a window of the previous 10 generations. In the LGA dockings, the pseudoSolis and Wets local search method was used, having a maximum of 300 iterations per local search; the probability of performing local search on an individual in the population was 0.06; the maximum number of consecutive successes or failures before doubling or halving the local search step size, r, was 4, in both cases; and the lower bound on r, the termination criterion for the local search, was 0.01.

TCR/Peptide/MHC Complex Structure. To make the whole TCR/peptide/MHC complex structure, superposition was done between the docked structure of the TCR/peptide and the docked structure of peptide/HLA or between the docked structure of the TCR/peptide and the crystal structure of the peptide/HLA complex. Then, the peptide structure was removed from the system. The structures obtained were further energy-minimized (MOE software).

ACKNOWLEDGMENTS. We thank M. Karplus for technical advice and D. Keskin for helpful comments. This work was supported by National Institutes of Health Research Grant 5RO1 AI049524 and National Multiple Sclerosis Society Award RG3796A3.

1. Bjorkman PJ, *et al.* (1987) The foreign antigen binding site and T cell recognition regions of class I histocompatibility antigens. *Nature* 329:512–518.
2. Brown JH, Jardetzky TS, Gorga JC, Stern LJ, Urban RG (1993) Three-dimensional structure of the human class II histocompatibility antigen HLA-DR1. *Nature* 364:33–39.
3. Rudolph MG, Stanfield RL, Wilson IA (2006) How TCRs bind MHCs, peptides, and coreceptors. *Annu Rev Immunol* 24:419–466.
4. Hedrick SM, Cohen DI, Nielsen EA, Davis MM (1984) Isolation of cDNA clones encoding T cell-specific membrane-associated proteins. *Nature* 308:149–153.
5. Yanagi Y, *et al.* (1984) A human T cell-specific cDNA clone encodes a protein having extensive homology to immunoglobulin chains. *Nature* 308:145–149.
6. Bentley GA, Boulot G, Karjalainen K, Mariuzza RA (1995) Crystal structure of the beta chain of a T cell antigen receptor. *Science* 267:1984–1987.
7. Mak TW (2007) The T cell antigen receptor. "The Hunting of the Snark." *Eur J Immunol* 37(Suppl 1):S83–S93.
8. Garboczi DN, *et al.* (1996) Structure of the complex between human T-cell receptor, viral peptide and HLA-A2. *Nature* 384:134–141.
9. Garcia KC, *et al.* (1996) An alphabeta T cell receptor structure at 2.5 A and its orientation in the TCR-MHC complex. *Science* 274:209–219.
10. Hahn M, Nicholson MJ, Pyrdol J, Wucherpfennig KW (2005) Unconventional topology of self peptide–major histocompatibility complex binding by a human autoimmune T cell receptor. *Nat Immunol* 6:490–496.

11. Wucherpfennig KW, *et al.* (1994) Clonal expansion and persistence of human T cells specific for an immunodominant myelin basic protein peptide. *J Immunol* 152:5581–5592.
12. Wucherpfennig KW, *et al.* (1994) Structural requirements for binding of an immunodominant myelin basic protein peptide to DR2 isotypes and for its recognition by human T cell clones. *J Exp Med* 179:279–290.
13. Morris GM, Goodsell DS, Huey R, Olson AJ (1996) Distributed automated docking of flexible ligands to proteins: Parallel applications of AutoDock 2.4. *J Comput Aided Mol Des* 10:293–304.
14. Stoddard BL, Koshland DE, Jr (1992) Prediction of the structure of a receptor-protein complex using a binary docking method. *Nature* 358:774–776.
15. Maynard J, *et al.* (2005) Structure of an autoimmune T cell receptor complexed with class II peptide-MHC: Insights into MHC bias and antigen specificity. *Immunity* 22:81–92.
16. Li Y, *et al.* (2005) Structure of a human autoimmune TCR bound to a myelin basic protein self-peptide and a multiple sclerosis-associated MHC class II molecule. *EMBO J* 24:2968–2979.
17. Hausmann S, Martin M, Gauthier L, Wucherpfennig KW (1999) Structural features of autoreactive TCR that determine the degree of degeneracy in peptide recognition. *J Immunol* 162:338–344.
18. Wucherpfennig KW, Hafler DA, Strominger JL (1995) Structure of human T-cell receptors specific for an immunodominant myelin basic protein peptide: Positioning of T-cell receptors on HLA-DR2/peptide complexes. *Proc Natl Acad Sci USA* 92:8896–8900.
19. Fechteler T, Dengler U, Schomberg D (1995) Prediction of Protein Three-Dimensional Structures in Insertion and Deletion Regions: A Procedure for Searching Databases of Representative Protein Fragments Using Geometric Scoring Criteria. *J Mol Biol* 253:114–131.
20. Levitt M (1992) Accurate Modeling of Protein Conformation by Automatic Segment Matching. *J Mol Biol* 226:507–533.
21. Hennecke J, Carfi A, Wiley DC (2000) Structure of a covalently stabilized complex of a human αβ T-cell receptor, influenza HA peptide and MHCII molecule, HLA-DR1. *EMBO J* 19:5611–5624.

IL-10 plays an important role as an immune-modulator in the pathogenesis of atopic diseases

MINAKO KAWAMOTO, EIKO MATSUI, HIDEO KANEKO, TOSHIYUKI FUKAO, TAKAHIDE TERAMOTO, KIMIKO KASAHARA and NAOMI KONDO

Department of Pediatrics, Graduate School of Medicine, Gifu University, Gifu, Japan

Received July 7, 2008; Accepted September 15, 2008

DOI: 10.3892/mmr_00000037

Abstract. Interleukin (IL)-10 has anti-inflammatory activities in various immune reactions and plays an important role in the regulation of immune diseases. In the present study, we examined the role of IL-10 in atopic diseases. Peripheral blood mononuclear cells (PBMCs) from healthy control subjects, patients with atopic dermatitis and patients with bronchial asthma were cultured with lipopolysaccharide (LPS). The production of IL-10, IL-12 or IFN-γ by PBMCs stimulated with LPS was measured. Next, we investigated whether the haplotype in the *IL-10* gene promoter region had an effect on the production of IL-10 by PBMCs. PBMCs from patients were cultured with phytohemagglutinin, to which recombinant human IL-10 had been added. IL-12, IFN-γ and IL-4 production by PBMCs was measured. ß-lactoglobulin (BLG)-specific T cell clones were cultured with BLG peptide (P-17), antigen-presenting cells and recombinant human IL-10. The antigen-induced proliferation of the T cell clones and cytokine production were assayed. Results demonstrated that IL-10 production by LPS-stimulated PBMCs was lower in atopic patients than in healthy control subjects. Three different haplotypes in the *IL-10* gene promoter region were detected. These haplotypes did not correlate with IL-10 production by PBMCs. IL-10 inhibited Th1 cytokine production by PBMCs, and also inhibited the antigen-induced proliferation of T cell clones and Th2 cytokine production. In conclusion, IL-10 inhibits both the production of Th1 and Th2 cytokines and the antigen-induced proliferation of T cell clones. Thus, IL-10 modulates other cytokines and plays an important role as an immune-modulator in the pathogenesis of atopic diseases.

Introduction

Interleukin (IL)-10, which is a homodimeric cytokine produced by activated monocytes, macrophages, mast cells and T cells, is deeply involved in the regulation of inflammatory responses and immune reactions. IL-10 was originally described as an inhibitory factor produced by murine Th2 cells that suppresses interferon-γ (IFN-γ) production by activated murine Th1 cells (1-3). Later, studies demonstrated IL-10 to be a potent inhibitor of monocyte and macrophage functions, suppressing the production of many pro-inflammatory cytokines and chemokines (4-7).

Several studies demonstrated that IL-10 has an important role in the pathogenesis of inflammatory bowel disease and autoimmune diseases, such as rheumatoid arthritis, systemic lupus erythematosus and multiple sclerosis (8,9). These diseases are called Th1-mediated diseases, as Th1 cytokines play a central role in their inflammation.

Recently, studies have revealed that IL-10 is associated with the pathogenesis of Th2-mediated diseases, such as allergic diseases. Therefore, we investigated the involvement of IL-10 in allergic reactions.

Materials and methods

Atopic patients and control subjects. Twelve healthy control subjects and 31 patients with atopic disease were studied. The serum IgE levels and radioallergosorbent test (RAST) scores of 12 healthy control subjects, 12 patients with atopic dermatitis (AD) and 19 patients with bronchial asthma (BA) are listed in Table I. AD was diagnosed according to the criteria of Haniffin, and BA according to the criteria of The American Thoracic Society. The healthy control subjects had a negative history of atopic disease, and their serum IgE levels were within normal limits for their age. They were moreover healthy and free of any acute infections at blood sampling. The subjects were randomly selected through our hospital, and informed consent was obtained from all subjects or their parents.

Cell preparation. PBMCs were isolated from the heparinized blood samples of healthy control subjects and atopic patients by gradient centrifugation using Ficoll-Paque (Pharmacia,

Correspondence to: Dr Minako Kawamoto, Department of Pediatrics, Graduate School of Medicine, Gifu University, 1-1 Yanagido, Gifu 501-1194, Japan
E-mail: mina@gifu-u.ac.jp

Abbreviations: AD, atopic dermatitis; BA, bronchial asthma; IL-10, interleukin-10; IL-12, interleukin-12; IFN-γ, interferon-γ; Th1, helper T cell type 1; Th2, helper T cell type 2; BLG, ß-lactoglobulin; PBMCs, peripheral blood mononuclear cells

Key words: interleukin-10, atopic dermatitis, bronchial asthma, peripheral blood mononuclear cells, T cell clone, *interleukin-10* gene

Uppsala, Sweden). PBMCs were suspended at a density of 10^6/ml in RPMI-1640 medium supplemented with 10% heat-inactive fetal calf serum, 2 mmol/l L-glutamine, 100 U/ml penicillin and 100 mg/μl streptomycin (10).

Cell culture. PBMCs (10^6/ml) were cultured with 1 μg/ml lipopolysaccharide (LPS) (Sigma, St. Louis, MO, USA) for 24 h in a volume of 1 ml in a round-bottom tube (Falcon 2059, Becton Dickinson Labware, Lincoln Park, NJ, USA) at 37°C in a humidified atmosphere containing 5% CO_2.

PBMCs (10^6/ml) from one randomly selected healthy control subject, one AD patient and three BA patients were cultured with 10 μg/ml phytohemagglutinin (PHA) (Gibco BRL, Grand Island, NY, USA) or 1 μg/ml LPS and recombinant human IL-10 (Genzyme, Minneapolis, MN, USA) at 0.1, 0.5, 1, 5, 10, 20 or 100 ng/ml for 24 h in a volume of 1 ml in a round-bottom tube.

Antigen-induced proliferative responses and cytokine production of BLG-specific T cell clones. ß-lactoglobulin (BLG)-specific T cell clones were used as described previously (11). The antigen-induced proliferation of the T cell clones was assayed by culturing T cells ($2x10^4$/well) in 96-well flat-bottomed culture plates with the BLG peptide (P-17) and 3000 cGy-irradiated autologous PBMCs ($1.5x10^5$/well) as antigen-presenting cells (APCs) and recombinant human IL-10, (0.1, 1, 10 or 100 ng/ml) or recombinant human TGF-ß, (0.001, 0.01, 0.1, 1 or 10 ng/ml). Cells were cultured for 72 h with 1 μCi/well of [^{3}H] TdR during the final 16-h period, and the incorporated radioactivity was measured by liquid scintillation counting. To assay cytokine production, culture supernatants in 96-well flat-bottomed tubes were spun to remove cells after the cultures and were stored at -80°C until used for assay.

Cytokine assays. IL-10 concentration was measured with a human IL-10 enzyme-linked immunosorbent assay (ELISA) kit (BioSource International, CA, USA) with a detection limit of 15.6 pg/ml. IL-12 concentration was measured with a human IL-12 ELISA kit (BioSource International) with a detection limit of 7.81 pg/ml. IFN-γ concentration was measured with a human IFN-γ ELISA kit (Ohtsuka, Tokyo, Japan) with a detection limit of 15.6 pg/ml, and IL-4 concentration was measured with a human IL-4 ultrasensitive ELISA kit (BioSource International) with a detection limit of 0.39 pg/ml. Lastly, IL-5 concentration was measured with a human IL-5 ELISA kit (Bio Source International) with a detection limit of 11.7 pg/ml.

Detection of polymorphisms in the IL-10 gene. Genomic DNA was extracted from neutrophils with a Sepagene kit (Sanko Junyaku, Tokyo, Japan). The promoter region and five exons of the *IL-10* gene (Gene Bank accession no. U16720) were amplified and sequenced using an ABI PRISM 377 DNA sequencer.

Statistical analyses. The significance of the differences between groups was analyzed using the Mann-Whitney U test. Probability (p) values <0.05 were considered statistically significant.

Table I. Clinical features of the 43 subjects.

	Age (years)	Gender	Diagnosis	Serum IgE (IU/ml)	RAST scores	
					HD	Derf
Control subjects						
1	11	M	Healthy	5.7	0	0
2	1	M	Healthy	5.9	0	0
3	1	F	Healthy	11.0	0	0
4	1	M	Healthy	15.0	0	0
5	1	M	Healthy	25.0	0	0
6	1	F	Healthy	29.1	0	1
7	6	F	Healthy	58.0	0	0
8	5	F	Healthy	70.0	0	0
9	2	M	Healthy	72.0	0	0
10	4	F	Healthy	98.3	1	0
11	5	M	Healthy	100.0	0	0
12	1	F	Healthy	110.0	0	0
Atopic patients						
1	1	M	AD	16.8	2	3
2	0	M	AD	236.0	0	0
3	3	M	AD	1,123.1	5	6
4	3	F	AD	2,024.7	6	6
5	1	M	AD	2,586.5	3	1
6	13	M	AD	2,769.0	3	3
7	1	M	AD	3,476.0	5	4
8	4	F	AD	3,782.6	6	6
9	3	F	AD	4,514.1	6	6
10	6	F	AD	5,500.0	6	6
11	5	M	AD	6,729.9	6	6
12	1	F	AD	14,666.3	3	3
13	5	M	BA	114.6	4	5
14	2	F	BA	127.6	4	4
15	2	F	BA	148.0	4	4
16	3	F	BA	251.4	5	5
17	7	F	BA	267.7	3	4
18	4	M	BA	300.0	0	0
19	11	M	BA	451.0	5	5
20	14	F	BA	484.0	5	5
21	10	M	BA	516.5	5	5
22	9	M	BA	517.5	6	6
23	3	F	BA	545.2	6	6
24	6	M	BA	616.3	1	1
25	9	M	BA	669.9	3	3
26	14	M	BA	839.0	5	5
27	8	M	BA	907.0	6	6
28	12	F	BA	1,581.6	2	2
29	8	M	BA	1,700.0	6	5
30	13	M	BA	3,063.9	6	6
31	9	F	BA	3,860.6	3	4

AD, atopic dermatitis; BA, bronchial asthma. M, male; F, female. HD, house dust; Derf, *Dermatofagoides farinae*.